Noname manuscript No.
(will be inserted by the editor)

A 3D Continuous Path Generation Method and Evaluation for FDM Process

Shusen Sun · Yuan Yao · Yunliang Jiang

Received: date / Accepted: date

Abstract Although continuous fiber reinforced polymer composites 3D printing has begun to be widely used, the algorithm of global continuous path planning and its performance have not been thoroughly explored. This paper presents a spatial continuous path planning method. Firstly, 2D connected regions are extracted from the sliced data of the model and the processing sequence is generated. Then 2D continuous fill pattern is constructed for each connected region. Finally, all connected regions are interconnected in the order of processing sequence to generate a global continuous tool path. Samples with different fill patterns, printing parameters and inter-layer relationship are fabricated and evaluated. The results show that the continuous path can avoid cutting operations and improve the mechanical properties of the printed model.

Keywords Additive manufacture · Tool path · Continuous fill pattern

1 Introduction

At present, Fused Deposition Manufacturing(FDM) is the most widely used and significant manufacturing method of additive manufacturing(AM). Semi-finished filaments are extruded layer by layer to build functional models [1, 2]. It allows to use a wide variety of thermoplastic materials, such as plastic, resin, or various composite materials and fiber reinforcements to make models. The 3D printed product is a typical composite structure. Materials, tool path, temperature, etc. are all factors that will affect the physical properties of the final product.

Among these factors, continuous path is the most cost-effective way to realize quality control. In conventional FDM process, a discontinuous tool path will cause a frequently on-off switching of the print nozzle, which has negatively impacting on quality and precision [3, 4]. The continuous printing path can reduce the drastic changes in the amount of material extrusion caused by the path interruption, make the material distribution more uniform that will improve the mechanics property of the printed model from a macroscopic perspective. Continuous tool path can also reduce the amount of travel time. In addition, it is more important for printing composites with long fibers to avoid designing complex extrusion heads. Therefore the machine need not to do frequent cutting operations, which will reduce printing costs and improve the quality and stability of fabrication.

The method of generating continuous tool path has received more and more attention. However, most of the current works are focused on the design of 2D continuous fill patterns, as well as the generation of 3D frame structures. There is still a lack of systematic analysis for the algorithm of global continuous path generation and its influence on the performance of the formed structures.

This paper realizes a path generation method that combines intra-layer continuity and inter-layer continuity to achieve a spatial continuous tool path. In the

Shusen Sun
Rapid Manufacturing Engineering Center, School of Mechatronical and Engineering Automation, Shanghai University, Shanghai 200444, China

Yuan Yao
Rapid Manufacturing Engineering Center, School of Mechatronical and Engineering Automation, Shanghai University, Shanghai 200444, China

bending test, results of different fill patterns are evaluated and compared.

2 Related Works

2.1 Slicing

The core idea of 3D printing is layered manufacturing. The slicing method is the key procedure to build layers and construct contours which affects surface quality and mechanical properties of the manufacturing model. The basic slicing method can be found from the reviews papers [5] and [6]. In these methods, uniform slicing is widely used in industry because its simple and more stable than adapt slicing.

To improve the efficiency of slicing large-scale triangular models, Huang et al. [7] implemented a hash-based fast indexing to improve the efficiency of slicing. Minetto et al. [8] reported a new method that sliced more than 10 times faster than Slic3r.

While support printing and removing is also time consuming. The advent of multi-axis printing technology has led researchers to experiment with a variety of more flexible slicing methods to reduce support. Dai et al. [9] developed a greedy scheme based algorithm to search the support free layers in non-horizontal direction. Wei et al. [10] also presented a stochastic method to partition 3D models and generated support-free fabrication for shell models. These methods provide a more flexible way of slicing, but material flow is always affected by gravity, lack of support will result in a decrease in surface quality.

2.2 Planar path planning

Fill pattern is another important parameter in FDM, which directly affects the quality of final products. Several researches focused on improving the product performance by changing the 2D fill patterns. The zigzag and its improved pattern [4] are widely adopted in today's 3D printers due to the simplicity. However, these zigzag patterns consist of many sharp turns which lead to more over-fill or under-fill of the filament. Yang et al. [11] proposed a contour-parallel tool path, which formed by iso-contours of the Euclidean distance transform. This fill pattern has better smoothness but is discontinuous. Jin et al. [12, 13] used different fill patterns to obtain the hybrid fills. The problem is that it is difficult to connect between the different fill patterns.

Spiral tool path has been widely applied for pocket machining [14]. Held and Spielberger [15] decomposed a 2D layer into spirallable pockets and machined each pocket following a separate, classical spiral pattern. Spiral tool path is less common for AM, because the adjacent two layers with similar fill path are difficult to form an interlaced pattern and this will reduce the density of the formation and affects the strength [16]. Zhao et al. [17] proposed a Fermat spirals based method for layered manufacturing, which can build long, low-curvature path on each slice. Similar methods are also used in subtractive manufacturing [18].

2.3 Spatial path planning

Various robotic fabrication systems have been studied in recent years, which provided additional degree-of-freedom (DOF) in motion so that the direction of materials accumulation can be changed during fabrication [9, 19, 20]. These works also made spatial path planning become more complicated.

In addition, generation of spatial tool path is also a popular field of investigation to improve the mechanical properties of the products by regulating the distribution of the materials in the model. Dong et al. [21] used a FDM machine with double nozzles to print Kevlar fibers reinforced composites(KFRCs) and analyzed the effect of carbon fiber reinforced method. Andrew N. Dickson et al. [22] studied the method of woven carbon fiber composites. In most of the current works, only the effect of local continuity of path on performance is concerned. The spatial continuous path generation and the related performance evaluation of the printed models are not discussed in depth.

3 Proposed method

Given a workpiece with complex geometries, it is impossible to achieve a fully continuous 3D path without any redundancy. Therefore, our strategy is to generate a spatial continuous path for the input model, while minimizing the post-processing workload. Our solution is divided into three steps. (1) Generate a global processing sequence according to the positional relationship among the 2D connected regions of each layer, in which the printing order of each connected area is determined; (2) A continuous fill path is constructed by connecting the fill spirals from each connected region in the order of the processing sequence; (3) The corresponding G-code is generated based on the continuous path and the device configuration. The overall framework is shown as Fig. 1.

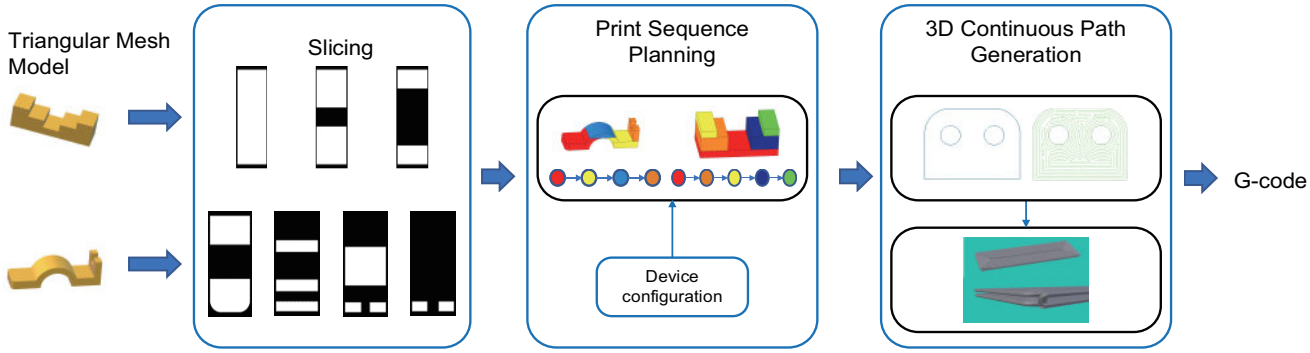

Fig. 1 Spatial continuous fill path generation

3.1 Slicing

Provided a triangle mesh model, the first task is to find the optimal printing direction of the model. Then We obtain the sliced data through slicing process and get the model contour of each layer. In this work, the method of slicing is Z-axis direction slicing because it is not only simple and stable, but also guarantees a good surface quality.

3.2 Processing sequence planning

To generate a continuous path in the spatial space and ensure the minimum workload of post-processing, We must determine the order of printing each 2D connected region of the model to ensure that each area is scanned only once. Therefore, the objective is to find a sequence $\mathbf{r} = [r_1, \ldots, r_2]$ that minimize the length of fill path. The problem can be defined as

$$\arg\min_{\mathbf{r}} \sum_{i=1}^{N} f_i(r_i) + \sum_{i=2}^{N} f_o(r_{i-1}, r_i) \quad s.t. \begin{cases} \mathbf{r} = [r_1, r_2, \ldots, r_n] \\ V = \sum_{i=1}^{N} g_a(r_i) \times \delta_i \end{cases} \tag{1}$$

Where r represents the connected region on each slice, V is the volume of input model, δ_i is the thickness of each layer. There are three functions, $f_i(r_i)$ is used to compute the length of infill path in each r, $f_o(r_{i-1}, r_i)$ calculates the length of the connecting line between r_{i-1} and r_i, and $g_a(r_i)$ gives the area of r_i. We use the 2D connected region r as an unit. If the current printed unit does not interfere with other units in the same layer, we can continue to print a unit in the next layer that is closest to the current unit. Unlike the traditional FDM, the print mode is converted from layer-by-layer to area-to-area. The details are presented in section 4.1.

3.3 Continuous path generation

Constructing a spatial continuous path consists of two steps. The first is to design an adapted fill pattern. We fill a continuous spiral inside each r, and the inlet and outlet of each filling spiral are placed close to each other. Then, according to the processing sequence generated previously, the spirals filled in each r are connected.

This method is not suitable for particularly complicated structures where structures are nested inside each other because it is difficult to remove the internal material in post-processing. But for most models, the path connecting each two connected regions can be wrapped around the outside of the bounding box, that makes it easy to remove material in the post processing.

4 Spatial continuous path

To clarify our algorithm of generating continuous path, in this section, we first give the concepts involved, and then describe the 2D and 3D continuous path generation process in detail according to the above steps.

The only concept to be clear is the connected region r that we mentioned above. As shown in Fig. 2(a), it refers to a simply connected domain or a non-simply connected domain on a sliced plane. We can fill it with a pattern of continuous path. The 2D continuous regions on the different slices are interconnected to form a continuous geometry in the z-direction. On the same slice, if there are two consecutive regions, the distance between them is large enough, and then it can be considered that there is no interference between the two geometries. This means that we can print one of the structures first and then the other without colliding with the structure already be fabricated, which is the basis of our approach.

4.1 Processing sequence

Given a 2D connected region r, its outer contour is defined by a set of points. We define the distance between two 2D connected regions as $d(r_1, r_2)$, which is Euclidean distance of the nearest pair of points on the boundaries of r_1 and r_2.

Assuming that the printing direction has been determined, if there is only one connected region in each slice, it is only necessary to connect all regions from the first slice to the last slice in order, otherwise we need a more complicated scanning strategy. This procedure is given in algorithm 1.

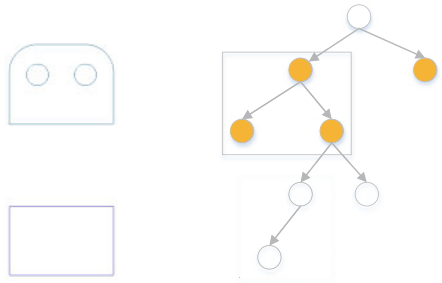

(a) Connected regions (b) Regions graph

Fig. 2 Connected regions extraction

The input variable D includes all 2D connected regions layer by layer, which are extracted from a set of slices of a triangle mesh model. As described above, slices are obtained according to the printing direction and thickness; see Fig. 2(a). Then connected region tree is constructed by 2D section contours(Fig. 2(b)). We traverse the connected region tree to get closed boundaries of each r. This operation is done on each layer, from the bottom to the top.

The output of algorithm 1 is **r** that contains a sequence of connected regions. Here we use (j, k) to index r instead of i. Where j represents the layer index, and k represents the region index in a layer. The algorithm contains two important decision processes. One is the function $is_interference$, which is used for interference testing between two connected regions, and the other is $Finds_urpported_regioni n_layer$, which detects if $r_{j,k}$ can be supported by a region in layer $j-1$.

4.2 2D continuous path

Given a connected region in a slice, a continuous path pattern must be selected and filled. As mentioned above, there are many continuous fill patterns exists, eg. Hilbert curve, zigzag, and so on. Here we prefer the spiral tool path because it produces smooth transitions and adapts to be filled in the connected region with complex geometry. The original idea is from the generation of parallel contours [23] and continuous spirals [17], but here a different strategy is deployed.

Algorithm 1 Processing sequence generation

```
GenSequence(D)
r ← ∅
r_{j,k} ← D.GetEnd()
while D is not empty do
    if NotInterfere(r_{j,k}) then
        r.Append(r_{j,k})
        D.RemoveItem(j,k)
        j ← j + 1
        r_{j,k} = D.FindSupportedRegion(j − 1, j)
        if NotFound then
            r_{j,k} ← D.GetEnd()
        end if
    else
        r_{m,l} ← D.GetEnd()
        if r_{m,l} == r_{j,k} then
            r.Append(r_{j,k})
            D.RemoveItem(j,k)
            r_{m,l} ← D.GetEnd()
        else
            if j <= m then
                r.Append(r_{j,k})
                D.RemoveItem(j,k)
            end if
            r_{j,k} ← r_{m,l}
        end if
    end if
end while
return r
```

As shown in Fig. 3(a), parallel contours are generated from the boundaries of the specified connected region. In order to generate a continuous path, we establish the adjacent relationship of each parallel contour by using the distance between two contours as a reference for the measure. If the distance between the two contours is close to the predefined offset, they are adjacent. A graph is created from this process. Since there are multiple boundary contours in a non-single connected region, this graph may containing cycles. Fig. 3(b) shows the corresponding directed graph of the parallel contours given by Fig. 3(a).

In these cycle structures, there are nodes with more than one parent nodes. Considering that assigning leaf nodes to any subgraph does not affect the efficiency of path generation. In the process of traversing the graph, we first delete one of the parent nodes, then detect whether the graph is still connected and reconstruct the graph. Finally, the directed graph structure is transformed into a graph without any circle. Which is shown in Fig. 4(b).

In this graph, the node containing the outermost outline is the root node, which can be converted into a

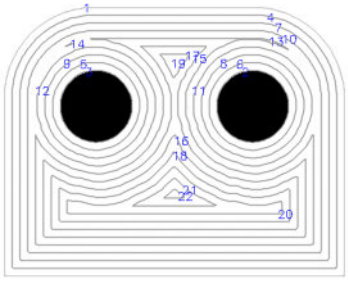

(a) Parallel contours

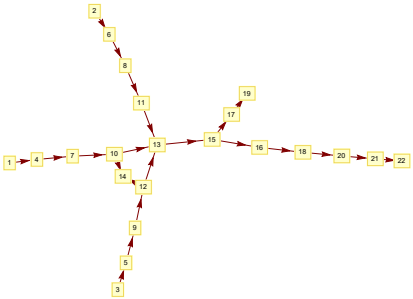

(b) Parallel contour graph

Fig. 3 Relationship of infill contours

minimum spanning tree(MST). Nodes with fewer than 2 edges can be grouped into one pocket, so we get the clustering structure shown in Fig. 4(a), and the neighboring relationships and the order of interconnection between the pockets.

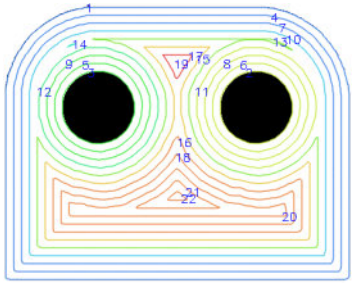

(a) Pocket groups

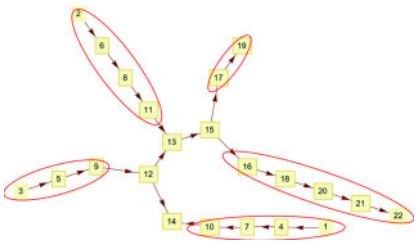

(b) Graph without cycle

Fig. 4 Pockets classification

According to the pocket division, we connect the parallel contours in a pocket into spirals (Fig. 4(a)), and interconnect each pocket by traversing the entire MST through deep priority search recursion. As shown in Fig. 6(b), a continuous path is generated for the current connected region.

The difficulty of this step consists of two aspects. First, the shape of the pocket is unpredictable. If the parallel contours are connected from the position with sharp features, the overlapping and crossing of the infill path are happened more than in smooth fields. Secondly, similar situations are existing when connecting two pockets. Therefore, how to choose the location of interconnection is an important issue.

To solve the first problem, we use the principal element analysis(PCA) method to analyze the macroscopic structure of the pocket. When a pocket with a narrow shape is encountered, priority is given to the position where the second greatest variance is located.

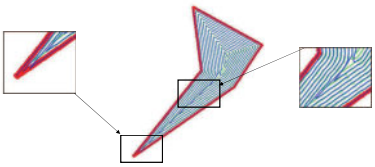

(a) Overlapping and crossing

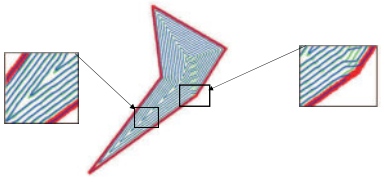

(b) Connection point relocation

Fig. 5 Illustration of continuous spiral path optimization by PCA

To solve the second problem, we use curvature scale space (CSS) [24] to locate the smooth position on the boundary. Then we search around this point to get another connection point. The CSS points on two spirals are given in Fig. 6(a), which represents the position where the curve curvature derivative equal to zero after Gaussian smoothing. At the macro level, the position of these points can be seen as a relatively smooth area on the curve. From Fig. 6(a) we can see that connecting in areas where curvature changes are small can avoid the problem of path intersection.

4.3 3D continuous path

The 2D continuous path and processing sequence implemented above are still continuous path optimization schemes in 2D plane. In order to realize 3D continuous

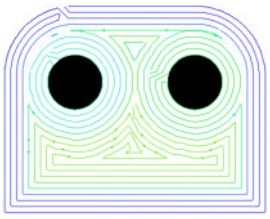

(a) Spiral in pocket

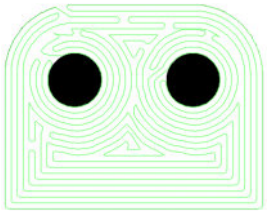

(b) Spirals interconnection

Fig. 6 Continuous fill pattern

path, we combine them and design a 3D continuous path scheme. The specific methods are as follows.

2D continuous path is the foundation of 3D continuous path. The continuous path in the 3D space realized in this paper is mainly aimed at the connection between layers to ensure the continuous printing. After printing the continuous paths in each layer, we connect the end point of the current layer with the starting point of the next layer by extruding continuous filament and lifting Z-axis, and then we get the 3D continuous paths; see Fig. 7. Moreover, we adjust the starting point of the continuous path in each layer, which reduces accumulation effect to improve the surface quality and forms different continuous path in different layers to achieve interleaving.

Fig. 7 Illustration of inter-layer continuous scheme

We optimize the printing scheme and get the processing sequence, which divide the model into different parts for printing. To realize continuous path, we designed the connection scheme between different parts. The path connection method between connected regions of different parts is to plan the connection path from the outside of the maximum bounding box of the structure so as to facilitate post-processing removal; see Fig. 8(b).

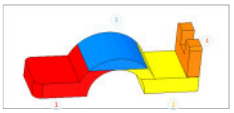

(a) Processing sequence

(b) Connection of different parts

Fig. 8 Illustration of processing sequence for keeping interlayer connection

5 Experiments and Evaluation

In order to demonstrate the effect of our method, we designed a series of samples with different infill path. These samples are fabricated with FDM machine and the physical properties are tested through the bending test. The surface quality is also evaluated and discussed with surface microscopy images.

5.1 Experiment setup

Eleven samples are selected in the experiments. Ten samples with PLA and one sample with carbon fiber reinforced nylon. Considered the long fibre reinforced material is involved in test samples, we adopt ISO 14125:1998 standard in the bending test. The dimension of test samples are 100mm × 3 mm × 25 mm.

Table 1 lists the detailed information and bending test results of all samples, where Cs is continuous path in our method, Fs is Fermat Spirals, Nf is normal fill pattern and Cp is contour-parallel. To investigate how continuous path influences on the mechanical properties, we considered four parameters: fill pattern, layer thickness, offset of continuous path and inter-layer relationship. Among them, sample 8 is carbon fiber sample printed by Markforged, others printed by desktop 3D printer. Printing results and analyses are based on the default printer.

Three-point loading method for bending test and bending test were measured by the microcomputer controlled electronic testing machine (WDW-1, SONGDUN Corp., China).

Test samples, dimensions and loading methods are shown in Fig. 9. The interleaving scheme is illustrated in Fig. 10. We choose different fill patterns for adjacent layers, such as zigzag and continuous path in our method, which forms interleaving between layers to improve the mechanical properties of the model.

Table 1 The design parameters of experimental and bending test results

Sample No.	Materials	Fill pattern	Layer thickness(mm)	Offset(mm)	Starting offset(Yes/No)	Bending strength (MPa)
1	PLA	Cs	0.20	0.40	Y	74.240
2	PLA	Cs	0.25	0.40	Y	70.758
3	PLA	Cs	0.30	0.40	Y	60.487
4	PLA	Cs	0.20	0.50	Y	65.986
5	PLA	Cs	0.20	0.60	Y	57.880
6	PLA	Cs	0.20	0.60	N	49.461
7	PLA	Nf	0.20	——	——	64.292
8	Carbon Fiber	——	0.125	——	——	50.405
9	PLA	Cs, zigzag	0.20	0.60	Y	62.071
10	PLA	Cp, zigzag	0.20	0.60	Y	59.250
11	PLA	zigzag	0.20	——	Y(0° /90°)	55.343

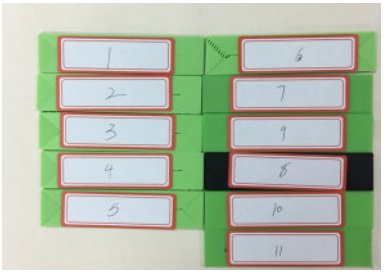

(a) The printed sample

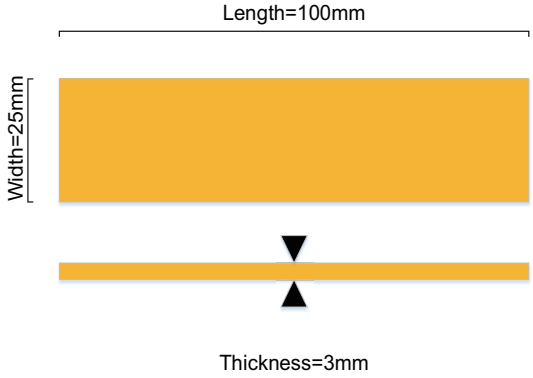

(b) Sample size

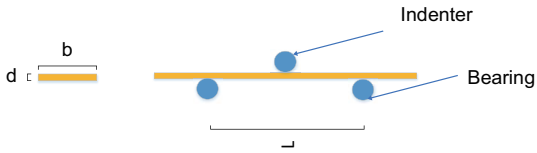

(c) Bending test

Fig. 9 Illustration of experiment setup

5.2 Experimental results and discussion

After each bending test, the corresponding bending stress-strain curves were calculated according to the bending test standards ISO 14125:1998. Bending stress σ and bending strain ϵ were calculated by formula 2 and 3. Where σ represents the stress in outer fibers at midpoint, ϵ is the strain in outer surface, P is the failure load, L is the support span, b and d are width of the sample and depth of the sample, and D is the maximum deflection of the center of the sample. The bending strength of the bending test are summarized in Table 1.

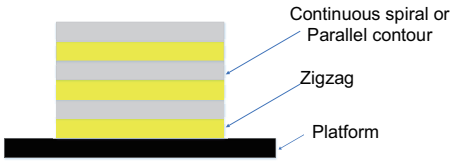

Fig. 10 Illustration of the interlacing relations of different layers

$$\sigma = 3PL/(2bd^2) \tag{2}$$

$$\epsilon = 6Dd/(L^2) \tag{3}$$

5.2.1 Evaluation of fill pattern

As shown in Fig. 11(d) and Table 1, the bending strength of sample No. 1 is the best and the bending strength is 74.240 MPa. Sample No. 8 is the worst which bending strength is 50.405 MPa. This is mainly due to the laying path of the fibers coincides with the transmission path of the force and the use of 3D continuous path for sample No. 1, which ensures continuous printing and smoothness of contour, thus reducing the negative impact of material accumulation on mechanical properties. Sample No. 8 is printed with carbon fibers reinforced nylon, including 16 layers of nylon and 8 layers of carbon fibers. Nylon materials mainly provide wrapping and bonding, while carbon fiber materials enhance mechanical properties. The poor test results are

mainly due to the weak radial mechanical properties of carbon fibers. The two peaks of stress-strain curve represent the resistance to deformation of nylon and carbon fibers after failure.

Surface quality results are shown in Fig. 11(a) - Fig. 11(c). The surface quality of the three samples is relatively smooth. The accumulation between contours of sample No. 1 is mainly due to the small offset of continuous path. The accumulation at the inflection points of samples No. 7 and No. 8 are mainly due to the rapid change of nozzle speed.

(a) Sample No. 1

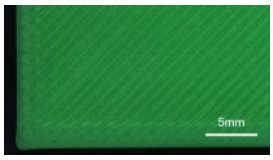

(b) Sample No. 7

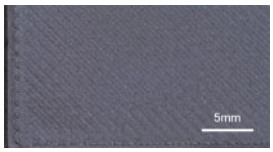

(c) Sample No. 8

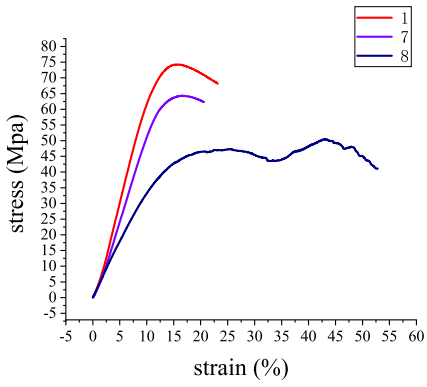

(d)

Fig. 11 Surface quality diagram and stress-strain diagram of samples No.1, No.7 and No.8.

5.2.2 Evaluation of layer thickness

The results of bending test for samples No. 1, No. 2 and No. 3 are shown in Fig. 12(d) and Table 1. Among them, sample No. 1 has the best mechanical properties whose bending strength is 74.240 MPa, bending strength of sample No. 2 is 70.758 MPa, sample No. 3 is the worst whose bending strength is 60.487 MPa. This is mainly because the smaller the thickness, the more the number of layers, the stronger to resist deformation.

Surface quality results are shown in Fig. 12(a) - Fig. 12(c). Sample No. 3 has the best surface quality and sample No. 1 has the worst surface quality. This is because the thickness of the layer is too small to extrude the molten material, so the accumulation between contours is obvious. The larger the thickness of the layer, the smaller the extrusion effect on the material. From surface quality results, the smaller the thickness, the worse the surface quality,this is because material accumulation in our method.

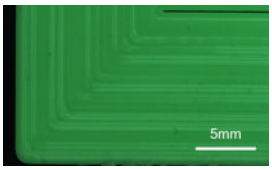

(a) Sample No. 1

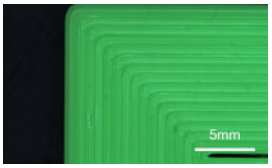

(b) Sample No. 2

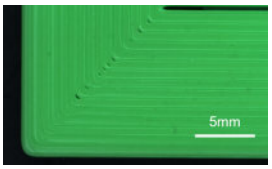

(c) Sample No. 3

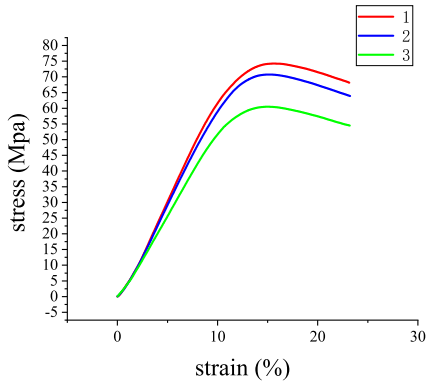

(d)

Fig. 12 Surface quality diagram and stress-strain diagram of samples No.1, No.2 and No.3.

5.2.3 Evaluation of contour offset

The results of the bending test for samples No. 1, No. 4 and No. 5 are shown in Fig. 13(d) and Table 1. Among them, sample No. 1 has the best mechanical properties whose bending strength is 74.240 MPa, bending strength of sample No. 4 is 65.986 MPa, sample No. 5 is the worst whose bending strength is 57.880 MPa. This is mainly because the thickness of 0.4mm corresponds to the diameter of nozzle, so contours of sample No. 1 are tight connected during the thermal change of the melted filament. Sample No. 5 has poor mechanical properties due to the large offset cannot form a strong connection between contours.

Surface quality results are shown in Fig. 13(a) - Fig. 13(c). Sample No. 5 has the best surface quality and sample No. 1 has the worst surface quality. The main reason is still that offset affects contour clearance. So sample No. 1 has obvious accumulation and poor surface quality.

5.2.4 Evaluation of inter-layer state

The results of bending test for samples No. 5 and No. 6 are shown in Fig. 14 and Table 1. Sample No. 5 has the best mechanical properties whose bending strength is 57.880 MPa and sample No. 6 is the worst whose bending strength is 49.461 MPa. This is mainly because sample No. 5 uses our continuous path method, which is continuous and interlaced between layers. Surface quality results are shown in Fig. 14(a) - Fig. 14(c). It can be seen that the surface quality of sample No. 5 is better. Sample No. 6 was filled with continuous path and the layers were connected in the same position, which resulted in gaps between contours. In addition, the side of sample No. 6 has more accumulation due to the same starting point position of all layers.

The results of bending test for samples No. 5, No. 9, No. 10 and No. 11 are shown in Fig. 15(e) and Table 1. Sample No. 9 has the best mechanical properties whose bending strength is 62.071 MPa and sample No. 11 is the worst whose bending strength is 55.343 MPa. Among them, the reason for fracture of No. 9, No. 10 and No. 11 sample is poor interlaminar connection and brittleness of mixed filling. Sample 9 has the best mechanical properties due to use zigzag and continuous path in this experiment. The mechanical properties of sample No. 10 are poor because the contours of sample No. 10 are parallel and there is no connection between contours. Although the inter-layer of sample No. 11 is staggered, the 90 degree is perpendicular to the direction of mechanical testing, so the mechanical properties of sample No. 11 are the worst. Surface quality results

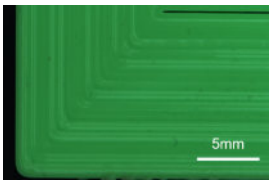

(a) Sample No. 1

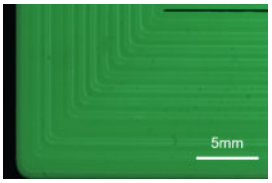

(b) Sample No. 4

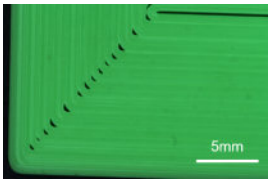

(c) Sample No. 5

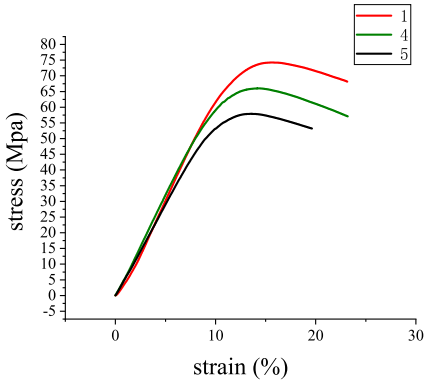

(d)

Fig. 13 Surface quality diagram and stress-strain diagram of samples No.1, No.4 and No.5.

are shown in Fig. 15(a) - Fig. 15(d). We can see that mixed fill has little effect on surface quality.

6 Conclusion

This paper presents a new method to generate continuous tool path for FDM process. We design this strategy based on traditional z-direction slices, and form a globally continuous 3D tool path by connecting the inner and inter-layer structures of each slice. This method can not only provide algorithm support for printing fiber reinforced polymer composites, but also adapt to the traditional FDM machine with popular polymer com-

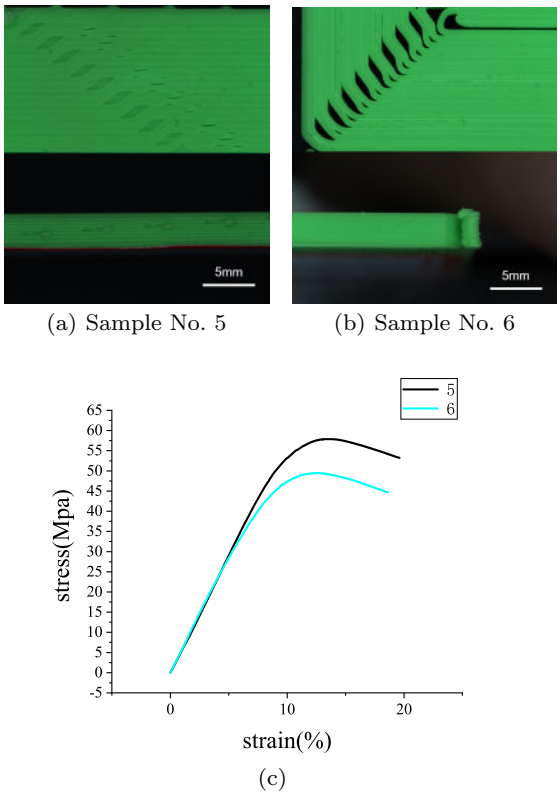

(a) Sample No. 5 (b) Sample No. 6

(c)

Fig. 14 Surface quality diagram and stress-strain diagram of samples No.5 and No.6.

posites to improve the strength of the workpiece in a specific direction without changing the design.

The current work still has several limitations in dealing with complex structures, inter-layer continuous path location , and fiber laying direction control. In the future work, we will test the method with more continuous filament fabrication samples and enhance the method to optimize the laying of fibers on the force transmission path.

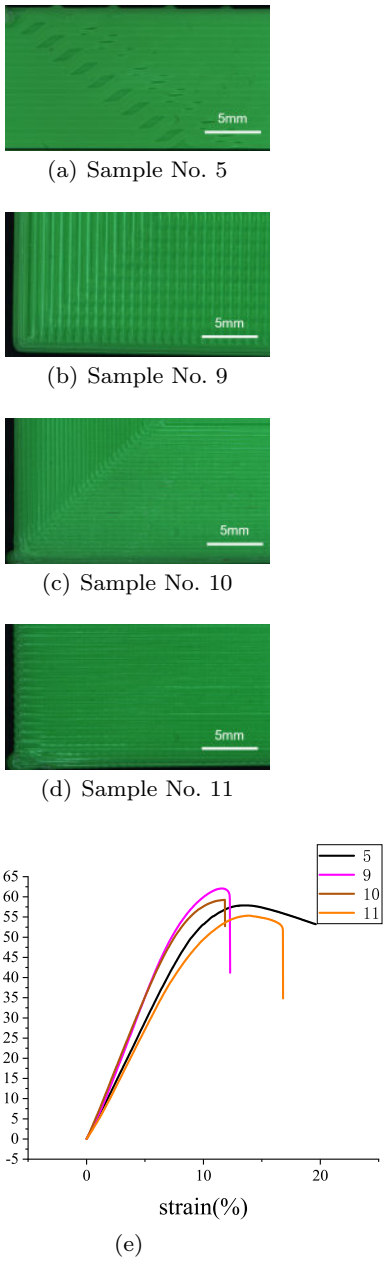

(a) Sample No. 5

(b) Sample No. 9

(c) Sample No. 10

(d) Sample No. 11

(e)

Fig. 15 Surface quality diagram and stress-strain diagram of samples No.5, No.9, No.10 and No.11.

References

1. Flaviana Calignano, Diego Manfredi, Elisa Paola Ambrosio, Sara Biamino, Mariangela Lombardi, Eleonora Atzeni, Alessandro Salmi, Paolo Minetola, Luca Iuliano, and Paolo Fino. Overview on additive manufacturing technologies. *Proceedings of the IEEE*, 105(4):593–612, 2017.
2. N. Mohan, P. Senthil, S. Vinodh, and N. Jayanth. A review on composite materials and process parameters optimisation for the fused deposition modelling process. *Virtual & Physical Prototyping*, 12(1):47–59, 2017.
3. Yu An Jin, Yong He, Jian Zhong Fu, Wen Feng Gan, and Zhi Wei Lin. Optimization of tool-path generation for material extrusion-based additive manufacturing technology. *Additive Manufacturing*, 1-4:32–47, 2014.
4. Donghong Ding, Zengxi Pan, Dominic Cuiuri, and Huijun Li. A tool-path generation strategy for wire and arc additive manufacturing. *International Journal of Advanced Manufacturing Technology*, 73 (1-4):173–183, 2014.
5. Pulak Mohan Pandey, N Venkata Reddy, and Sanjay G Dhande. Slicing procedures in layered manufacturing: a review. *Rapid prototyping journal*, 9

(5):274–288, 2003.
6. Wei Gao, Yunbo Zhang, Devarajan Ramanujan, Karthik Ramani, Yong Chen, Christopher B Williams, Charlie CL Wang, Yung C Shin, Song Zhang, and Pablo D Zavattieri. The status, challenges, and future of additive manufacturing in engineering. *Computer-Aided Design*, 69:65–89, 2015.
7. Xiaohu Huang, Yuan Yao, and Qingxi Hu. Research on the rapid slicing algorithm for nc milling based on stl model. In *Asian Simulation Conference*, pages 263–271. Springer, 2012.
8. Rodrigo Minetto, Neri Volpato, Jorge Stolfi, Rodrigo MMH Gregori, and Murilo VG Da Silva. An optimal algorithm for 3d triangle mesh slicing. *Computer-Aided Design*, 92:1–10, 2017.
9. Chengkai Dai, Charlie C. L. Wang, Chenming Wu, Sylvain Lefebvre, and Yong Jin Liu. Support-free volume printing by multi-axis motion. *ACM Transactions on Graphics*, 37(4):1–14, 2018.
10. X. Wei, S. Qiu, L. Zhu, R. Feng, Y. Tian, J. Xi, and Y. Zheng. Toward support-free 3d printing: A skeletal approach for partitioning models. *IEEE Transactions on Visualization and Computer Graphics*, 24(10):2799–2812, 2018.
11. Y. Yang, H. T. Loh, J. Y. H. Fuh, and Y. G. Wang. Equidistant path generation for improving scanning efficiency in layered manufacturing. *Rapid Prototyping Journal*, 8(1):30–37, 2002.
12. G. Q. Jin, W. D. Li, and L. Gao. An adaptive process planning approach of rapid prototyping and manufacturing. *Robotics & Computer Integrated Manufacturing*, 29(1):23–38, 2013.
13. G. Q. Jin, W. D. Li, L. Gao, and K. Popplewell. A hybrid and adaptive tool-path generation approach of rapid prototyping and manufacturing for biomedical models. *Computers in Industry*, 64(3): 336–349, 2013.
14. Fei Ren, Yuwen Sun, and Dongming Guo. Combined reparameterization-based spiral toolpath generation for five-axis sculptured surface machining. *International Journal of Advanced Manufacturing Technology*, 40(7-8):760–768, 2009.
15. Martin Held and Christian Spielberger. A smooth spiral tool path for high speed machining of 2d pockets. *Computer-Aided Design*, 41(7):539–550, 2009.
16. Jürgen Stampfl and Markus Hatzenbichler. *Additive Manufacturing Technologies*. 2014.
17. Haisen Zhao, Baoquan Chen, Fanglin Gu, Qi Xing Huang, Jorge Garcia, Chen Yong, Changhe Tu, Bedrich Benes, Zhang Hao, and Daniel Cohen-Or. Connected fermat spirals for layered fabrication. *Acm Transactions on Graphics*, 35(4):1–10, 2016.
18. Haisen Zhao, Hao Zhang, Shiqing Xin, Yuanmin Deng, Changhe Tu, Wenping Wang, Daniel Cohen-Or, and Baoquan Chen. Dscarver: Decompose-and-spiral-carve for subtractive manufacturing. *ACM Transactions on Graphics (Special Issue of SIGGRAPH)*, 37(4):Article No. 137, 2018.
19. Rundong Wu, Huaishu Peng, François Guimbretière, and Steve Marschner. Printing arbitrary meshes with a 5dof wireframe printer. *ACM Trans. Graph.*, 35(4):101:1–101:9, July 2016. ISSN 0730-0301.
20. Chenming Wu, Chengkai Dai, Guoxin Fang, Yong Jin Liu, and Charlie C. L. Wang. Robofdm: A robotic system for support-free fabrication using fdm. In *2017 IEEE International Conference on Robotics and Automation (ICRA)*, 2017.
21. Guoying Dong, Yunlong Tang, Dawei Li, and Yaoyao Fiona Zhao. Mechanical properties of continuous kevlar fiber reinforced composites fabricated by fused deposition modeling process. *Procedia Manufacturing*, 26:774 – 781, 2018. 46th SME North American Manufacturing Research Conference, NAMRC 46, Texas, USA.
22. Andrew N. Dickson, Keri-Ann Ross, and Denis P. Dowling. Additive manufacturing of woven carbon fibre polymer composites. *Composite Structures*, 206:637 – 643, 2018.
23. Martin Held, Gábor Lukács, and László Andor. Pocket machining based on contour-parallel tool paths generated by means of proximity maps. *Computer-Aided Design*, 26(3):189–203, 1994.
24. Farzin Mokhtarian and Miroslaw Bober. Robust image corner detection through curvature scale space. In *Curvature Scale Space Representation: Theory, Applications, and MPEG-7 Standardization*, pages 215–242. Springer, 2003.